



# Interpretation of chiral symmetry breaking and octupole correlations in $^{124}\text{Cs}$ by the reflection-asymmetric triaxial particle rotor model

Y. Y. Wang  and S. Q. Zhang \**State Key Laboratory of Nuclear Physics and Technology, School of Physics, Peking University, Beijing 100871, China*

(Received 1 May 2020; accepted 17 August 2020; published 3 September 2020)

The positive-parity doublet bands with configuration  $\pi h_{11/2} \otimes \nu h_{11/2}$  and negative-parity bands with  $\pi h_{11/2} \otimes \nu(g_{7/2}d_{5/2})$  observed in  $^{124}\text{Cs}$ , and the possibility of multiple chiral doublets ( $M\chi D$ ) with octupole correlations are investigated using the reflection-asymmetric triaxial particle rotor model. The calculated excitation energies, energy staggering parameters, and the electromagnetic transitional probabilities are in good agreement with the data available and satisfy the expected features of chiral doublet bands. The angular momentum geometry and its evolution with spin are studied with the angular momentum components and the *azimuthal plot*. In comparison with a typical chiral vibration pattern for the positive-parity doublet bands, a transient static chirality around  $I = 12\hbar$  is shown for the calculated negative-parity doublet bands.

DOI: [10.1103/PhysRevC.102.034303](https://doi.org/10.1103/PhysRevC.102.034303)

## I. INTRODUCTION

Chiral symmetry and its breaking is of general interest in multiple fields of natural science. The concept of chirality in atomic nuclei was first proposed by Frauendorf and Meng in 1997 [1]. Since then, many efforts have been made to understand nuclear chirality and its spontaneous breaking; see reviews [2–7].

In the laboratory frame, the restoration of chiral symmetry that spontaneously breaks in the intrinsic frame can be manifested as a pair of nearly degenerate  $\Delta I = 1$  bands with the same parity, i.e., chiral doublet bands [1]. In 2006, based on the self-consistent covariant density functional theory [8], a phenomenon named multiple chiral doublets ( $M\chi D$ ) is suggested, which shows more than one pair of chiral doublet bands can exist in one single nucleus [9]. Experimental evidence for  $M\chi D$  has been reported in  $^{133}\text{Ce}$  [10], followed by  $^{103}\text{Rh}$  [11],  $^{78}\text{Br}$  [12],  $^{136}\text{Nd}$  [13],  $^{195}\text{Tl}$  [14],  $^{135}\text{Nd}$  [15], and  $^{131}\text{Ba}$  [16]. Up to now, at least 60 candidate chiral bands in around 50 nuclei (including 11  $M\chi D$  candidates [10–20]) have been reported in the  $A \approx 80, 100, 130$ , and 190 mass regions [21].

On the theoretical side, various approaches have been developed to investigate nuclear chirality, such as the particle rotor model (PRM) [1,22–26], the titled axis cranking (TAC) approach [1,27–30], the TAC approach with the random phase approximation (TAC + RPA) [31,32] and the collective Hamiltonian (TAC + CH) [33–35], the interacting boson-fermion-fermion model (IBFFM) [36], the generalized coherent state model [20], and the projected shell model (PSM) [37–41].

One should note that the  $M\chi D$  phenomenon reflects the diversity of chiral symmetry breaking in one nucleus and

provides the unique opportunity to investigate the correlations between different chiral doublet bands. In 2016, the  $M\chi D$  candidates were reported in  $^{78}\text{Br}$ , in which eight strong electric dipole ( $E1$ ) transitions linking the positive- and negative-parity chiral bands were observed [12]. The observation shows an example of the  $M\chi D$  bands with octupole correlations and indicates the simultaneously spontaneous breaking of chiral and space-reflection symmetries in atomic nuclei. In order to investigate the  $M\chi D$  in  $^{78}\text{Br}$ , a reflection-asymmetric triaxial particle rotor model (RAT-PRM) was recently developed [42,43] and the experimental observables such as the excitation energies, energy staggering parameters,  $B(M1)/B(E2)$  ratios, and  $B(E1)/B(E2)$  ratios were interpreted [42].

It is interesting to find more cases of the  $M\chi D$  bands with octupole correlations. In the  $A \approx 130$  mass region, the nucleus  $^{124}\text{Cs}$  deserves more attention. In  $^{124}\text{Cs}$ , a pair of positive-parity doublet bands with configuration  $\pi h_{11/2} \otimes \nu h_{11/2}$  has been observed experimentally [44,45] and further interpreted as chiral doublet bands by using the triaxial PRM [46] and triaxial PSM [38]. In particular, the electromagnetic transitional properties deduced from the lifetime measurements agree well with the characteristic pattern required for chiral symmetry breaking for these bands [47]. For the negative-parity bands, one  $\Delta I = 1$  band with configuration  $\pi h_{11/2} \otimes \nu(g_{7/2}d_{5/2})$  has been observed in Refs. [44,45]. Another two negative-parity  $\Delta I = 2$  bands were observed with the possible interpretation as the yrare  $\pi h_{11/2} \otimes \nu(g_{7/2}d_{5/2})$  configuration by the IBFFM and the cranked-shell model (CSM), while the CSM also provided another possible configuration  $\pi h_{11/2} \otimes \nu d_{3/2}$  [45]. A recent study extended the two  $\Delta I = 2$  bands with the suggestion of odd neutron in the *sd* orbitals by the cranked Nilsson-Strutinsky model [48]. Remarkably, the evidences for the octupole correlations between the positive- and negative-parity bands have been presented [44,47–49].

In this work, the newly developed RAT-PRM is applied to investigate the possibility of the observed positive- and

\*sqzhang@pku.edu.cn

negative-parity bands in  $^{124}\text{Cs}$  as  $M\chi D$  bands with octupole correlations. The excitation energies, energy staggering parameters, and the electromagnetic properties of the observed positive- and negative-parity bands will be analyzed. Since the chiral geometry of the positive-parity doublet bands has been already studied by the triaxial PRM [46], we will focus on the interband  $E1$  transitions between the positive- and negative-parity bands and the possible chiral geometry in the negative-parity bands. The model is briefly introduced in Sec. II and the numerical details are presented in Sec. III. The calculated results for the doublet bands, such as energy spectra, electromagnetic transitions, the angular momentum components, and the *azimuthal plot* are discussed in Sec. IV. A summary is given in Sec. V.

## II. THEORETICAL FRAMEWORK

The detailed RAT-PRM formalism can be found in Ref. [42]. The total Hamiltonian is

$$\hat{H} = \hat{H}_{\text{intr.}}^p + \hat{H}_{\text{intr.}}^n + \hat{H}_{\text{core}}, \quad (1)$$

where  $\hat{H}_{\text{intr.}}^{p(n)}$  is the intrinsic Hamiltonian for valence protons (neutrons) in a reflection-asymmetric triaxially deformed potential, and  $\hat{H}_{\text{core}}$  is the Hamiltonian of a reflection-asymmetric triaxial rotor.

The core Hamiltonian can be generalized straightforwardly from the reflection-asymmetric axial rotor in Ref. [50],

$$\hat{H}_{\text{core}} = \sum_{k=1}^3 \frac{\hat{R}_k^2}{2\mathcal{J}_k} + \frac{1}{2}E(0^-)(1 - \hat{P}_c), \quad (2)$$

in which  $\hat{R}_k = \hat{I}_k - \hat{J}_{pk} - \hat{J}_{nk}$ , and  $\hat{R}_k$ ,  $\hat{I}_k$ ,  $\hat{J}_{pk}$ , and  $\hat{J}_{nk}$  are the angular momentum operators for the core, the nucleus, and the valence protons and neutrons, respectively. For the moments of inertia (MOIs), the type of irrotational flow is adopted  $\mathcal{J}_k = \mathcal{J}_0 \sin^2(\gamma - 2k\pi/3)$ . In the last term, the core parity splitting parameter  $E(0^-)$  can be viewed as the excitation energy of the virtual  $0^-$  state [50], and the core parity operator  $\hat{P}_c$  is the product of the single-particle parity operator  $\hat{\pi}$  and the total parity operator  $\hat{P}$ .

The intrinsic Hamiltonian for valence nucleons is [24,51,52]

$$\hat{H}_{\text{intr.}}^{p(n)} = \sum_{\nu>0} (\varepsilon_{\nu}^{p(n)} - \lambda)(a_{\nu}^{\dagger}a_{\nu} + a_{\bar{\nu}}^{\dagger}a_{\bar{\nu}}) - \frac{\Delta}{2} \sum_{\nu>0} (a_{\nu}^{\dagger}a_{\bar{\nu}}^{\dagger} + a_{\bar{\nu}}a_{\nu}), \quad (3)$$

where  $\lambda$  denotes the Fermi energy,  $\Delta$  is the pairing gap parameter, and  $|\bar{\nu}\rangle$  is the time-reversal state of  $|\nu\rangle$ . The single-particle energy  $\varepsilon_{\nu}^{p(n)}$  is obtained by diagonalizing the Hamiltonian  $\hat{H}_{\text{s.p.}}^{p(n)}$ , which has the form of a Nilsson Hamiltonian [53],

$$\hat{H}_{\text{s.p.}}^{p(n)} = -\frac{1}{2}\hbar\omega_0\nabla^2 + V(r; \theta, \varphi) + Cl \cdot s + D[I^2 - (I^2)_N], \quad (4)$$

with the kinetic energy  $-\frac{1}{2}\hbar\omega_0\nabla^2$ , the reflection-asymmetric triaxially deformed potential  $V(r; \theta, \varphi)$  [42], the spin-orbit term  $Cl \cdot s$ , and the standard  $D[I^2 - (I^2)_N]$  term [54].

The Hamiltonian  $\hat{H}$  is diagonalized numerically in the symmetrized strong-coupled basis with good parity and

angular momentum [42], which gives rise to the eigenvalues and eigen wave functions. By using the resulting wave functions, one can also calculate the reduced electromagnetic transition probabilities, the expectation values of angular momentum components, and so on [42].

## III. NUMERICAL DETAILS

In the present RAT-PRM calculations for the two pairs of positive- and negative-parity doublet bands in  $^{124}\text{Cs}$ , as a reasonable choice, the adopted quadrupole deformation parameters  $(\beta_2, \gamma)$  are  $(0.25, 33.8^\circ)$ . These values are obtained from the configuration-fixed triaxial covariant density functional theory (CDFT) calculation [9] with density functional PC-PK1 [55] for the positive-parity configuration  $\pi h_{11/2} \otimes \nu h_{11/2}$  and are close to  $(0.27, 28.6^\circ)$  obtained for the negative-parity one  $\pi h_{11/2} \otimes \nu(g_{7/2}d_{5/2})$ . To consider the effect of octupole correlations, an octupole deformation parameter  $\beta_3 = 0.03$  is used.

For the intrinsic part, the reflection-asymmetric triaxial Nilsson Hamiltonian (4) with the parameters  $\kappa, \mu$  in Ref. [56] is solved in the harmonic oscillator basis [57]. The Fermi energies in Eq. (3) are chosen for proton and neutron as  $\lambda_p = 44.8$  MeV and  $\lambda_n = 48.5$  MeV, corresponding to the  $\pi h_{11/2}[m_z = 1/2]$  and  $\nu h_{11/2}[m_z = 7/2]$  orbitals, respectively. The single-particle space available to the odd nucleon was truncated to 13 levels, with six above and six below the Fermi level. Increasing the size of the single-particle space does not influence the band structure in the present work. The pairing correlation is taken into account by the empirical pairing gap formula  $\Delta = 12/\sqrt{A}$  MeV. For the core part, it turns out that a configuration-dependent MOI is necessary to reproduce the experimental energy spectra, which is  $\mathcal{J}_0 = 20 \hbar^2/\text{MeV}$  for positive-parity doublet bands and  $34 \hbar^2/\text{MeV}$  for negative-parity doublet bands. A larger  $\mathcal{J}_0$  for negative-parity doublet bands is consistent with the larger quadrupole deformation parameter  $\beta_2$  obtained for configuration  $\pi h_{11/2} \otimes \nu(g_{7/2}d_{5/2})$ , but the detail dependence of MOI on different configurations deserves further investigation. The core parity splitting parameter  $E(0^-) = 1$  MeV is used. For the calculations of the electromagnetic transitions, the empirical intrinsic dipole moment  $Q_{10} = (3/4\pi)R_0Z\beta_{10}$  and quadrupole moment  $Q_0 = (3/\sqrt{5\pi})R_0^2Z\beta_2$  are taken with  $R_0 = 1.2A^{1/3}$  fm, and gyromagnetic ratios for the collective rotor, protons, and neutrons are given by  $g_R = Z/A$ ,  $g_{p(n)} = g_l + (g_s - g_l)/(2l + 1)$  [54,58].

## IV. RESULTS AND DISCUSSION

The excitation energies and the energy staggering parameters  $S(I) = [E(I) - E(I-1)]/2I$  calculated by the RAT-PRM for the positive- and negative-parity doublet bands in  $^{124}\text{Cs}$  are shown in Fig. 1 in comparison with the experimental data [45,47]. Here, following the notation in Ref. [47], the positive-parity doublet bands are labeled by bands 1 and 2, and the negative-parity ones by bands 3 and 4. Note that the experimental data of band 4 are only of the odd-spin sequence.

As shown in Fig. 1(a), the calculated excitation energies well reproduce the data for the positive-parity doublet bands

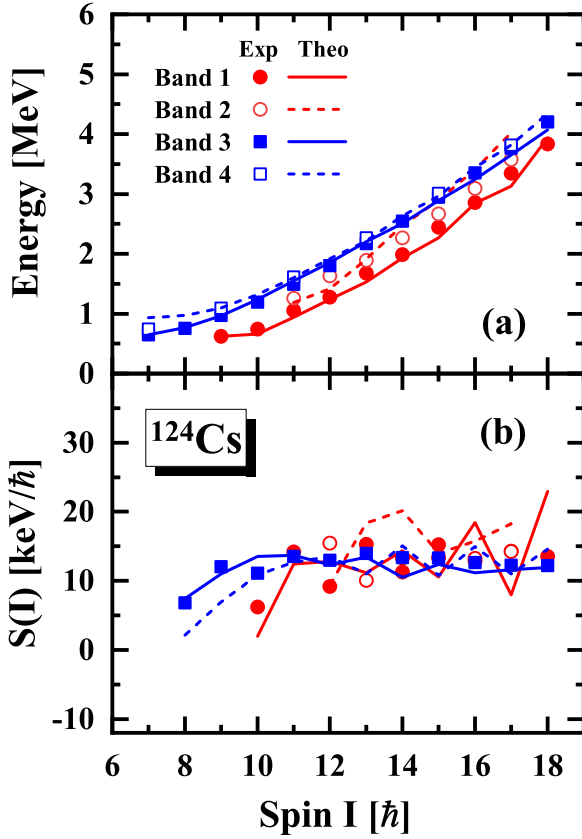


FIG. 1. The excitation energies  $E(I)$  (a) and the energy staggering parameters  $S(I) = [E(I) - E(I - 1)]/2I$  (b) for the positive-parity doublet bands 1 and 2 as well as for the negative-parity doublet bands 3 and 4 in  $^{124}\text{Cs}$  by RAT-PRM (lines) in comparison with the experimental data [45,47] (symbols). The calculated excitation energies in Fig. 1(a) are shifted to coincide with the experimental energy at  $I = 9\hbar$  in band 1 for positive-parity bands and at  $I = 7\hbar$  in band 3 for negative-parity bands.

and the negative-parity bands. For the observed spin range of  $11\hbar \leq I \leq 17\hbar$  for the positive-parity doublet bands and  $7\hbar \leq I \leq 18\hbar$  for the negative-parity bands, the calculated average energy differences are 0.49 and 0.14 MeV, respectively. The calculated results show that the negative-parity doublet bands have better level degeneracy than the positive-parity ones.

As shown in Fig. 1(b), at first glance, the calculated energy staggering parameters  $S(I)$  well reproduce the data available for the positive-parity doublet bands and the negative-parity band 3 not only in the magnitude of the  $S(I)$  values but also in the small amplitude of the staggering of  $S(I)$ . For the positive-parity doublet bands, however, the staggering of the calculated  $S(I)$  shows an antiphase with that of the experimental  $S(I)$  at a number of spins. Considering that the configuration of the positive-parity doublet bands has been firmly assigned as  $\pi h_{11/2} \otimes \nu h_{11/2}$  [44–48], the reason for the antiphase may result from the fact that the detailed changes of configuration mixing with spin are difficult to reproduce with a specific calculation. Nevertheless, both the calculated and experimental  $S(I)$  values show only a slight staggering with spin for the positive-parity doublet bands and a slighter

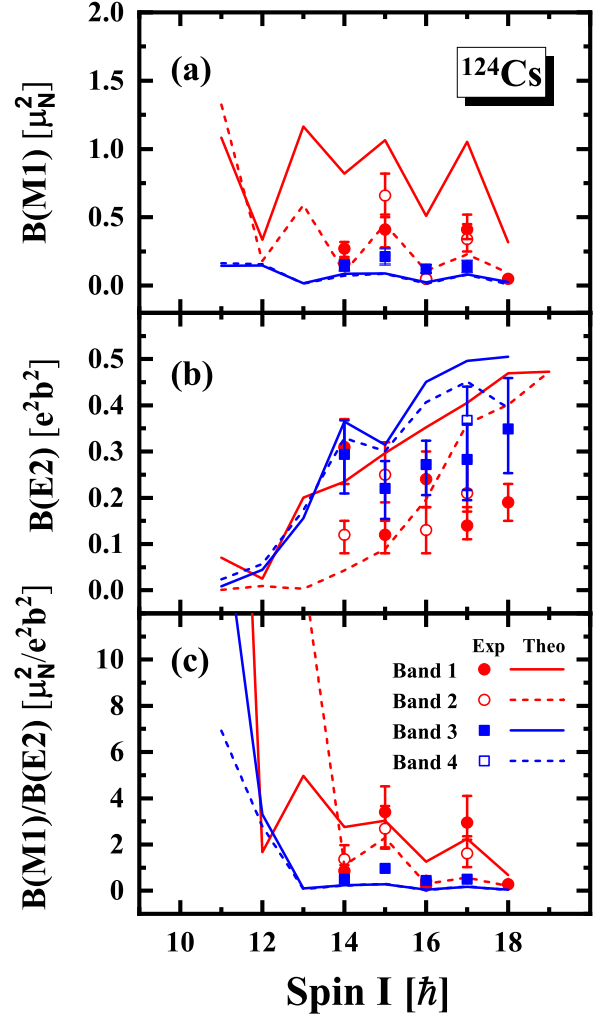


FIG. 2. The  $B(M1)$  (a),  $B(E2)$  (b), and  $B(M1)/B(E2)$  (c) values calculated by the RAT-PRM for the positive- and negative-parity doublet bands in  $^{124}\text{Cs}$  in comparison with the data available [47].

staggering for the negative-parity ones. As commented in Ref. [59], the independence of the quantity  $S(I)$  with spin in the chiral region can serve as an important criterion for chirality. Therefore, from both the staggering parameter  $S(I)$  and the energy differences between doublet bands, the calculated negative-parity doublet bands 3 and 4 coincide with the criteria for chirality even better than the positive-parity doublet bands 1 and 2.

The calculated  $B(M1)$ ,  $B(E2)$ , and  $B(M1)/B(E2)$  ratios for the two pairs of doublet bands are shown in Fig. 2, in comparison with the data available [47]. As shown in Figs. 2(a) and 2(b), the order of magnitude and the trend of the experimental  $B(M1)$  and  $B(E2)$  values are well reproduced for both positive- and negative-parity bands. Both theoretical and experimental  $B(M1)$  values show clear odd-even staggering behavior. However, for both  $B(M1)$  and  $B(E2)$  values, the calculated difference between positive-parity doublet bands is larger than that between negative-parity bands, as well as that between experimental positive-parity doublet bands. As shown in Ref. [24], the deviation from an ideal particle-hole

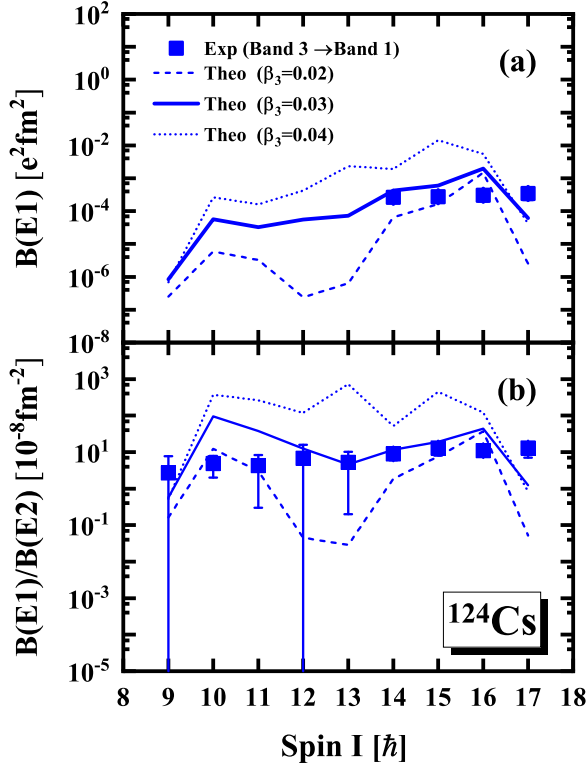


FIG. 3. The calculated  $B(E1)$  values of the interband  $E1$  transitions (band 3  $\rightarrow$  band 1) (a) and the corresponding ratios over the  $B(E2)$  values of the intraband  $E2$  transitions (band 3) (b) in  $^{124}\text{Cs}$  in comparison with the data available [47].

configuration may lead to an obvious difference in the calculated  $B(M1)$  and  $B(E2)$  values between chiral doublet bands. In contrast the valence neutron of the negative-parity bands sitting in the top of the  $(g_{7/2}d_{5/2})$  subshell, the valence neutron of the positive-parity bands sits in the middle of the  $h_{11/2}$  subshell, deviating from an ideal hole configuration. In addition, the electromagnetic transitional strengths depend sensitively on the detailed intrinsic wave functions, which may account for the deviations of the calculation from experiment.

As shown in Fig. 2(c), the magnitude, the odd-even staggering, and also the similarity between doublet bands of the  $B(M1)/B(E2)$  ratios are reproduced quite well for the observed spin region. In Ref. [46], the electromagnetic transition properties for the positive-parity doublet bands including  $B(M1)/B(E2)$  and  $B(M1)_{\text{in}}/B(M1)_{\text{out}}$  have been discussed, which still hold true in the present calculations. The electromagnetic transition properties such as the odd-even staggering of  $B(M1)$  values and the similarity between doublet bands also indicate the chiral nature for the calculated negative-parity doublet bands.

With the consideration of the octupole degree of freedom, the electric dipole transition probabilities  $B(E1)$  between the positive- and negative-parity bands can be obtained by using the present RAT-PRM calculation. In Fig. 3, the calculated interband  $E1$  transitions (band 3  $\rightarrow$  1) and the corresponding ratios over the  $B(E2)$  values of the intraband  $E2$  transitions (band 3) are shown in comparison with the data available

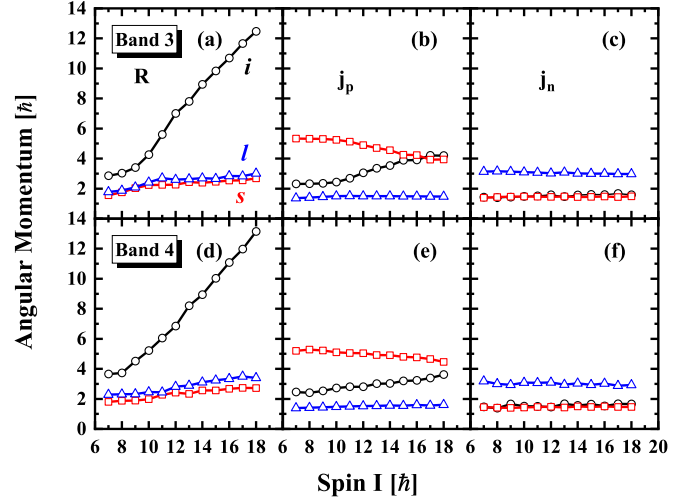


FIG. 4. The angular momentum components along the intermediate ( $i$ , circles), short ( $s$ , squares), and long ( $l$ , triangles) axes for the core  $R_k = \langle \hat{R}_k^2 \rangle^{1/2}$  [(a), (d)], valence proton  $j_{pk} = \langle \hat{j}_{pk}^2 \rangle^{1/2}$  [(b), (e)], and valence neutron  $j_{nk} = \langle \hat{j}_{nk}^2 \rangle^{1/2}$  [(c), (f)] in RAT-PRM for the negative-parity doublet bands 3 and 4 in  $^{124}\text{Cs}$ .

[47]. As shown in Figs. 3(a) and 3(b), the calculated  $B(E1)$  and  $B(E1)/B(E2)$  values with  $\beta_3 = 0.03$  adopted in the present work satisfactorily agree with the experimental data. To investigate the influence of the octupole deformation, the RAT-PRM calculations with  $\beta_3 = 0.02$  and  $0.04$  have been performed. It is found that there is no significant influence on the excitation energies, staggering parameters,  $B(M1)$  and  $B(E2)$  values by changing  $\beta_3$  from  $0.02$  to  $0.04$ , while the  $B(E1)$  and  $B(E1)/B(E2)$  ratios sensitively depend on the octupole deformation parameter  $\beta_3$ . As shown in Figs. 3(a) and 3(b), the calculated  $B(E1)$  and  $B(E1)/B(E2)$  values can be enhanced up to three orders of magnitude by changing  $\beta_3$  from  $0.02$  to  $0.04$ .

In addition to the physical observables, the particle rotor model also provides us a tool to examine the chiral geometry of the doublet bands [6,24,25,39]. For the positive-parity doublet bands in  $^{124}\text{Cs}$ , the chiral geometry including the expectation values, the effective angles, and the probability distributions of the angular momentum has been investigated by the triaxial PRM, which indicates that these doublet bands mainly correspond to a typical chiral vibration pattern [46]. Similar examination of the chiral geometry has been performed by the present RAT-PRM and consistent results with Ref. [46] are obtained for the positive-parity doublet bands. In the following, the examination of the chiral geometry for the negative-parity doublet bands is presented in detail.

In Fig. 4, the angular momentum components for the core  $R_k = \langle \hat{R}_k^2 \rangle^{1/2}$ , the valence proton  $j_{pk} = \langle \hat{j}_{pk}^2 \rangle^{1/2}$ , and the valence neutron  $j_{nk} = \langle \hat{j}_{nk}^2 \rangle^{1/2}$  ( $k = 1, 2, 3$ ) are presented for the negative-parity doublet bands. For the triaxial deformation  $\gamma = 33.8^\circ$  adopted here, the intrinsic axes 1, 2, and 3 are respectively the intermediate ( $i$ ), short ( $s$ ), and long ( $l$ ) axes, and the relation of the corresponding moments of inertia is  $\mathcal{J}_1 > \mathcal{J}_2 > \mathcal{J}_3$ . Therefore, as shown in Fig. 4 for negative-parity doublet bands, the collective core angular momentum

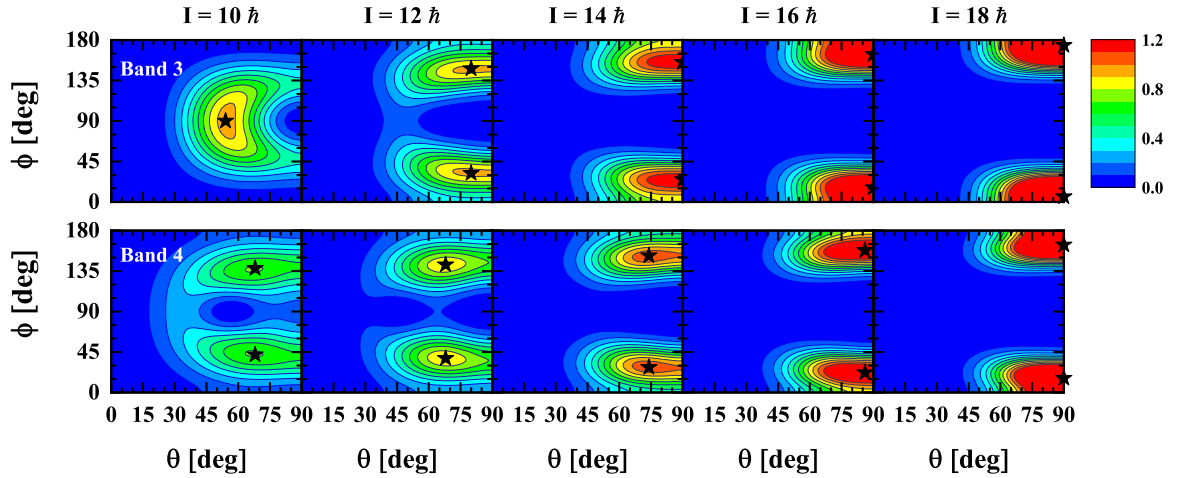


FIG. 5. The *azimuthal plot*, i.e., the probability profile for the orientation of the angular momentum on the  $(\theta, \phi)$  plane (see text), calculated at spins  $I = 10, 12, 14, 16,$  and  $18\hbar$ , for the negative-parity doublet bands 3 and 4 in  $^{124}\text{Cs}$ . The maximum in each plot is labeled as a black star.

mainly aligns along the  $i$  axis, because it has the largest moment of inertia. The angular momentum of the valence proton mainly aligns along the  $s$  axis, and the alignment of the valence neutron along the  $l$  axis is significant. To be more precise,  $j_p \sim 5.5\hbar$  along the  $s$  axis,  $j_n \sim 3\hbar$  along  $l$  axis, and  $R \sim 3\hbar - 13\hbar$  along  $i$  axis. This forms the chiral geometry for the negative-parity doublet bands. As the total angular momentum increases,  $R$  increases gradually,  $j_n$  remains almost unchanged, while  $j_p$  moves gradually toward the  $i$  axis. The difference between the proton and neutron alignments may result from the fact that the Coriolis alignment effects are weaker for the neutron in the relatively low- $j$  ( $g_{7/2}d_{5/2}$ ) shell.

In Fig. 5, the calculated *azimuthal plot* [39,60], i.e., the probability profile for the orientation of the angular momentum on the  $(\theta, \phi)$  plane, for the negative-parity doublet bands at  $I = 10, 12, 14, 16,$  and  $18\hbar$  is shown. The polar angle  $\theta$  is the angle between the angular momentum and the intrinsic 3-axis, and the azimuthal angle  $\phi$  is the angle between the projection of the angular momentum on the intrinsic 1-2 plane and the 1-axis.

For spin  $I = 10\hbar$ , the profile for the orientation of the angular momentum for band 3 has a single peak at  $(\theta = 54^\circ, \phi = 90^\circ)$ , which suggests that the angular momentum stays within the 2-3 plane. The profile for band 4 shows a node at  $(\theta = 54^\circ, \phi = 90^\circ)$ , with two peaks at  $(\theta = 68^\circ, \phi = 42^\circ)$  and  $(\theta = 68^\circ, \phi = 138^\circ)$ . The existence of the node and the two peaks supports that the state in band 4 can be interpreted as a 1-phonon chiral vibration across the 2-3 plane on the state in band 3.

For spin  $I = 12\hbar$ , the *azimuthal plots* for bands 3 and 4 are similar. Two peaks corresponding to aplanar orientations are found, i.e.,  $(\theta = 80^\circ, \phi = 32^\circ)$  and  $(\theta = 80^\circ, \phi = 148^\circ)$  for band 3 and  $(\theta = 68^\circ, \phi = 38^\circ)$  and  $(\theta = 68^\circ, \phi = 142^\circ)$  for band 4, respectively. These features could be understood as a realization of static chirality, where the nonvanishing distribution for  $\theta = 90^\circ$  and  $\phi = 90^\circ$  reflects the tunneling between the left- and right-handed configurations.

For spins  $I = 14, 16,$  and  $18\hbar$ , the two peaks for the *azimuthal plots* for band 3 appear at  $\theta = 90^\circ$  with  $\phi$  moving close to  $0^\circ$  and  $180^\circ$ , respectively. As a result, the total angular momentum is more likely to lie in the 1-2 plane and moves toward the 1-axis, which is in accordance with the dominance of rotation around the 1-axis reflected in Fig. 4. The process shows the disappearance of chiral geometry in band 3 and the onset of principal axis rotation. The peaks for the *azimuthal plots* for band 4 locate at  $(\theta = 74^\circ, \phi = 28^\circ)$  and  $(\theta = 74^\circ, \phi = 152^\circ)$  for  $I = 14\hbar$  and  $(\theta = 86^\circ, \phi = 22^\circ)$  and  $(\theta = 86^\circ, \phi = 158^\circ)$  for  $I = 16\hbar$ , which indicate the chiral vibration across the 1-2 plane on the states in band 3. For  $I = 18\hbar$ , the locations of peaks for band 4 become  $(\theta = 90^\circ, \phi = 16^\circ)$  and  $(\theta = 90^\circ, \phi = 164^\circ)$ , presenting a planar rotation and indicating a termination of chiral vibration.

Therefore, in comparison with a typical chiral vibration pattern for the positive-parity doublet bands [46], a transient static chirality around  $I = 12\hbar$  is shown for the negative-parity doublet bands. The feature presented by chiral geometry is consistent with the judgment obtained from the energy differences between doublet bands and the staggering parameter that the negative-parity doublet bands coincide with the criteria for chirality even better than the positive-parity doublet bands. The difference between the two pairs of doublet bands may be understood by the deviation of their configurations from an ideal particle-hole case. For the positive-parity doublet bands, the configuration is  $\pi h_{11/2} \otimes \nu h_{11/2}$  with a proton particle sitting in the bottom of the  $h_{11/2}$  shell and a neutron sitting in the middle of the  $h_{11/2}$  shell [46]. For the negative-parity doublet bands, the configuration is more close to an ideal particle-hole case with a neutron hole sitting in the top of the  $(g_{7/2}d_{5/2})$  shell, although the proton configuration is the same as that of the positive-parity doublet bands.

Finally, a few remarks on the experimental observation of band 4 are appropriate. Although the RAT-PRM suggests the calculated negative-parity doublet bands to be chiral partners and the calculated odd-spin sequence of yrare band is in good agreement with the experimental band 4, it is unlikely to

interpret the observed band 4 as the yrare partner of band 3 with configuration  $\pi h_{11/2} \otimes \nu(g_{7/2}d_{5/2})$ . As shown in Fig. 1, the calculated band 4 shows almost no signature splitting with spin; however, no signature degenerate partner of the experimental band 4 was observed yet, even though a nearly degenerate signature partner would be much easier to observe than the reported even-spin sequences in Refs. [45,48,49]. Therefore, compared with the yrare configuration of band 3, another configuration  $\pi h_{11/2} \otimes \nu s_{1/2}$  is more realistic for band 4 as suggested in Ref. [48]. In this circumstance, more efforts are necessary to identify the possible chiral partner band of band 3 and to confirm the prediction of  $M\chi D$  with octupole correlations in  $^{124}\text{Cs}$ .

## V. SUMMARY

In summary, the reflection-asymmetric triaxial particle rotor model is applied to investigate the observed positive-parity doublet bands with configuration  $\pi h_{11/2} \otimes \nu h_{11/2}$  and negative-parity bands with  $\pi h_{11/2} \otimes \nu(g_{7/2}d_{5/2})$  in  $^{124}\text{Cs}$ , and to examine their chiral geometry. The calculated excitation energies, the energy staggering parameters, and the electromagnetic transitional probabilities reasonably reproduce the data for both the positive- and negative-parity bands. It is found that the  $B(E1)$  and  $B(E1)/B(E2)$  ratios sensitively depend on the octupole deformation parameter  $\beta_3$  and the experimental data can be satisfactorily reproduced by  $\beta_3 = 0.03$ .

The angular momentum geometry and its evolution with spin  $I$  for the two pairs of doublet bands in  $^{124}\text{Cs}$  calculated by RAT-PRM have been investigated. Consistent results with Ref. [46] are obtained for the positive-parity doublet bands, which indicate that they mainly correspond to a typical chiral vibration pattern. For the negative-parity doublet bands, by examining the angular momentum components and the *azimuthal plot*, the chiral geometry and evolution have been presented which show a transient static chirality around  $I = 12\hbar$ . Finally, these two calculated pairs of positive- and negative-parity doublet bands in  $^{124}\text{Cs}$  may be interpreted as a candidate of  $M\chi D$  bands with octupole correlations. So far the yrare partner for the negative-parity chiral bands is not observed, and more efforts are still necessary to confirm the prediction of  $M\chi D$  with octupole correlations in  $^{124}\text{Cs}$ .

## ACKNOWLEDGMENTS

Fruitful discussions with Prof. Jie Meng and Prof. Pengwei Zhao are gratefully acknowledged. This work was partly supported by the National Natural Science Foundation of China (Grants No. 11875075, No. 11935003, No. 11975031, and No. 11621131001), the National Key R&D Program of China (Contracts No. 2018YFA0404400 and No. 2017YFE0116700), the State Key Laboratory of Nuclear Physics and Technology, Peking University (No. NPT2020ZZ01), and the China Postdoctoral Science Foundation under Grant No. 2020M670014.

- 
- [1] S. Frauendorf and J. Meng, *Nucl. Phys. A* **617**, 131 (1997).  
 [2] S. Frauendorf, *Rev. Mod. Phys.* **73**, 463 (2001).  
 [3] J. Meng and S. Q. Zhang, *J. Phys. G* **37**, 064025 (2010).  
 [4] J. Meng and P. W. Zhao, *Phys. Scr.* **91**, 053008 (2016).  
 [5] A. A. Raduta, *Prog. Part. Nucl. Phys.* **90**, 241 (2016).  
 [6] K. Starosta and T. Koike, *Phys. Scr.* **92**, 093002 (2017).  
 [7] S. Frauendorf, *Phys. Scr.* **93**, 043003 (2018).  
 [8] Edited by J. Meng, *Relativistic Density Functional for Nuclear Structure*, International Review of Nuclear Physics Vol. 10 (World Scientific, Singapore, 2016).  
 [9] J. Meng, J. Peng, S. Q. Zhang, and S.-G. Zhou, *Phys. Rev. C* **73**, 037303 (2006).  
 [10] A. D. Ayangeakaa, U. Garg, M. D. Anthony, S. Frauendorf, J. T. Matta, B. K. Nayak, D. Patel, Q. B. Chen, S. Q. Zhang, P. W. Zhao, B. Qi, J. Meng, R. V. F. Janssens, M. P. Carpenter, C. J. Chiara, F. G. Kondev, T. Lauritsen, D. Seweryniak, S. Zhu, S. S. Ghugre, and R. Palit, *Phys. Rev. Lett.* **110**, 172504 (2013).  
 [11] I. Kuti, Q. B. Chen, J. Timár, D. Sohler, S. Q. Zhang, Z. H. Zhang, P. W. Zhao, J. Meng, K. Starosta, T. Koike, E. S. Paul, D. B. Fossan, and C. Vaman, *Phys. Rev. Lett.* **113**, 032501 (2014).  
 [12] C. Liu, S. Y. Wang, R. A. Bark, S. Q. Zhang, J. Meng, B. Qi, P. Jones, S. M. Wyngaardt, J. Zhao, C. Xu, S.-G. Zhou, S. Wang, D. P. Sun, L. Liu, Z. Q. Li, N. B. Zhang, H. Jia, X. Q. Li, H. Hua, Q. B. Chen, Z. G. Xiao, H. J. Li, L. H. Zhu, T. D. Bucher, T. Dinoko, J. Easton, K. Juhász, A. Kamblawe, E. Khaleel, N. Khumalo, E. A. Lawrie, J. J. Lawrie, S. N. T. Majola, S. M. Mullins, S. Murray, J. Ndayishimye, D. Negi, S. P. Noncolela, S. S. Ntshangase, B. M. Nyakó, J. N. Orce, P. Papka, J. F. Sharpey-Schafer, O. Shirinda, P. Sithole, M. A. Stankiewicz, and M. Wiedeking, *Phys. Rev. Lett.* **116**, 112501 (2016).  
 [13] C. M. Petrache, B. F. Lv, A. Astier, E. Dupont, Y. K. Wang, S. Q. Zhang, P. W. Zhao, Z. X. Ren, J. Meng, P. T. Greenlees, H. Badran, D. M. Cox, T. Grahn, R. Julin, S. Juutinen, J. Konki, J. Pakarinen, P. Papadakis, J. Partanen, P. Rakhila, M. Sandzelius, J. Saren, C. Scholey, J. Sorri, S. Stolze, J. Uusitalo, B. Cederwall, O. Aktas, A. Ertoprak, H. Liu, S. Matta, P. Subramaniam, S. Guo, M. L. Liu, X. H. Zhou, K. L. Wang, I. Kuti, J. Timár, A. Tucholski, J. Srebrny, and C. Andreoiu, *Phys. Rev. C* **97**, 041304(R) (2018).  
 [14] T. Roy, G. Mukherjee, M. Asgar, S. Bhattacharyya, S. Bhattacharya, C. Bhattacharya, S. Bhattacharya, T. Ghosh, K. Banerjee, S. Kundu, T. Rana, P. Roy, R. Pandey, J. Meena, A. Dhal, R. Palit, S. Saha, J. Sethi, S. Thakur, B. Naidu, S. Jadav, R. Dhonti, H. Pai, and A. Goswami, *Phys. Lett. B* **782**, 768 (2018).  
 [15] B. F. Lv, C. M. Petrache, Q. B. Chen, J. Meng, A. Astier, E. Dupont, P. Greenlees, H. Badran, T. Calverley, D. M. Cox, T. Grahn, J. Hilton, R. Julin, S. Juutinen, J. Konki, J. Pakarinen, P. Papadakis, J. Partanen, P. Rakhila, P. Ruotsalainen, M. Sandzelius, J. Saren, C. Scholey, J. Sorri, S. Stolze, J. Uusitalo, B. Cederwall, A. Ertoprak, H. Liu, S. Guo, M. L. Liu, J. G. Wang, X. H. Zhou, I. Kuti, J. Timár, A. Tucholski, J. Srebrny, and C. Andreoiu, *Phys. Rev. C* **100**, 024314 (2019).  
 [16] S. Guo, C. Petrache, D. Mengoni, Y. H. Qiang, Y. P. Wang, Y. Y. Wang, J. Meng, Y. K. Wang, S. Q. Zhang, P. W. Zhao, A. Astier, J. G. Wang, H. L. Fan, E. Dupont, B. F. Lv, D. Bazzacco, A. Boso, A. Goasduff, F. Recchia, D. Testov, F.

- Galtarossa, G. Jaworski, D. Napoli, S. Riccetto, M. Siciliano, J. J. Valiente-Dobon, M. L. Liu, G. S. Li, X. H. Zhou, Y. H. Zhang, C. Andreoiu, F. H. Garcia, K. Ortner, K. Whitmore, A. Atac-Nyberg, T. Back, B. Cederwall, E. A. Lawrie, I. Kuti, D. Sohler, T. Marchlewski, J. Srebrny, and A. Tucholski, *Phys. Lett. B* **807**, 135572 (2020).
- [17] A. A. Hecht, C. W. Beausang, H. Amro, C. J. Barton, Z. Berant, M. A. Caprio, R. F. Casten, J. R. Cooper, D. J. Hartley, R. Krücken, D. A. Meyer, H. Newman, J. R. Novak, N. Pietralla, J. J. Ressler, A. Wolf, N. V. Zamfir, J.-Y. Zhang, and K. E. Zyranski, *Phys. Rev. C* **68**, 054310 (2003).
- [18] J. Li, S. Q. Zhang, and J. Meng, *Phys. Rev. C* **83**, 037301 (2011).
- [19] B. Qi, H. Jia, N. B. Zhang, C. Liu, and S. Y. Wang, *Phys. Rev. C* **88**, 027302 (2013).
- [20] A. A. Raduta, A. H. Raduta, and C. M. Petrache, *J. Phys. G* **43**, 095107 (2016).
- [21] B. W. Xiong and Y. Y. Wang, *At. Data Nucl. Data Tables* **125**, 193 (2019).
- [22] J. Peng, J. Meng, and S. Q. Zhang, *Phys. Rev. C* **68**, 044324 (2003).
- [23] T. Koike, K. Starosta, and I. Hamamoto, *Phys. Rev. Lett.* **93**, 172502 (2004).
- [24] S. Q. Zhang, B. Qi, S. Y. Wang, and J. Meng, *Phys. Rev. C* **75**, 044307 (2007).
- [25] B. Qi, S. Q. Zhang, J. Meng, S. Y. Wang, and S. Frauendorf, *Phys. Lett. B* **675**, 175 (2009).
- [26] Q. B. Chen, B. F. Lv, C. M. Petrache, and J. Meng, *Phys. Lett. B* **782**, 744 (2018).
- [27] V. I. Dimitrov, S. Frauendorf, and F. Döna, *Phys. Rev. Lett.* **84**, 5732 (2000).
- [28] P. Olbratowski, J. Dobaczewski, J. Dudek, and W. Płóciennik, *Phys. Rev. Lett.* **93**, 052501 (2004).
- [29] P. Olbratowski, J. Dobaczewski, and J. Dudek, *Phys. Rev. C* **73**, 054308 (2006).
- [30] P. W. Zhao, *Phys. Lett. B* **773**, 1 (2017).
- [31] S. Mukhopadhyay, D. Almed, U. Garg, S. Frauendorf, T. Li, P. V. M. Rao, X. Wang, S. S. Ghugre, M. P. Carpenter, S. Gros, A. Hecht, R. V. F. Janssens, F. G. Kondev, T. Lauritsen, D. Seweryniak, and S. Zhu, *Phys. Rev. Lett.* **99**, 172501 (2007).
- [32] D. Almed, F. Döna, and S. Frauendorf, *Phys. Rev. C* **83**, 054308 (2011).
- [33] Q. B. Chen, S. Q. Zhang, P. W. Zhao, R. V. Jolos, and J. Meng, *Phys. Rev. C* **87**, 024314 (2013).
- [34] Q. B. Chen, S. Q. Zhang, P. W. Zhao, R. V. Jolos, and J. Meng, *Phys. Rev. C* **94**, 044301 (2016).
- [35] X. H. Wu, Q. B. Chen, P. W. Zhao, S. Q. Zhang, and J. Meng, *Phys. Rev. C* **98**, 064302 (2018).
- [36] S. Brant, D. Tonev, G. De Angelis, and A. Ventura, *Phys. Rev. C* **78**, 034301 (2008).
- [37] K. Hara and Y. Sun, *Int. J. Mod. Phys. E* **04**, 637 (1995).
- [38] G. H. Bhat, R. N. Ali, J. A. Sheikh, and R. Palit, *Nucl. Phys. A* **922**, 150 (2014).
- [39] F. Q. Chen, Q. B. Chen, Y. A. Luo, J. Meng, and S. Q. Zhang, *Phys. Rev. C* **96**, 051303(R) (2017).
- [40] F. Q. Chen, J. Meng, and S. Q. Zhang, *Phys. Lett. B* **785**, 211 (2018).
- [41] Y. K. Wang, F. Q. Chen, P. W. Zhao, S. Q. Zhang, and J. Meng, *Phys. Rev. C* **99**, 054303 (2019).
- [42] Y. Y. Wang, S. Q. Zhang, P. W. Zhao, and J. Meng, *Phys. Lett. B* **792**, 454 (2019).
- [43] Y. Y. Wang, X. H. Wu, S. Q. Zhang, P. W. Zhao, and J. Meng, *Sci. Bull.* (2020), doi: 10.1016/j.scib.2020.08.028.
- [44] J. Lu, Y. Liu, L. Yin, G. Zhao, F. Zhang, X. Li, R. Meng, Z. Wang, Y. Ma, Z. Wang, J. Huo, X. Wu, S. Wen, G. Li, and C. Yang, *Phys. Rev. C* **62**, 057304 (2000).
- [45] A. Gizon, J. Timár, J. Gizon, B. Weiss, D. Barneoud, C. Foin, J. Genevey, F. Hannachi, C. F. Liang, A. Lopez-Martens, P. Paris, B. M. Nyako, L. Zolnai, J. C. Merdinger, and S. B. V. Paar, *Nucl. Phys. A* **694**, 63 (2001).
- [46] S. Y. Wang, B. Qi, and D. P. Sun, *Phys. Rev. C* **82**, 027303 (2010).
- [47] K. Selvakumar, A. K. Singh, C. Ghosh, P. Singh, A. Goswami, R. Raut, A. Mukherjee, U. Datta, P. Datta, S. Roy, G. Gangopadhyay, S. Bhowal, S. Muralithar, R. Kumar, R. P. Singh, and M. K. Raju, *Phys. Rev. C* **92**, 064307 (2015).
- [48] A. K. Singh, A. Basu, S. Nag, H. Hübel, J. Domscheit, I. Ragnarsson, A. Al-Khatib, G. B. Hagemann, B. Herskind, D. R. Elema, J. N. Wilson, R. M. Clark, M. Cromaz, P. Fallon, A. Görger, I.-Y. Lee, D. Ward, and W. C. Ma, *Phys. Rev. C* **97**, 024323 (2018).
- [49] D. Yang, J.-B. Lu, Y.-Z. Liu, L.-L. Wang, K.-Y. Ma, C.-D. Yang, D.-K. Han, Y.-X. Zhao, Y.-J. Ma, L.-H. Zhu, X.-G. Wu, and G.-S. Li, *Chin. Phys. Lett.* **26**, 082101 (2009).
- [50] G. A. Leander and R. K. Sheline, *Nucl. Phys. A* **413**, 375 (1984).
- [51] I. Hamamoto, *Nucl. Phys. A* **271**, 15 (1976).
- [52] I. Hamamoto and B. Mottelson, *Phys. Lett. B* **127**, 281 (1983).
- [53] S. G. Nilsson, *Dan. Mat. Fys. Medd.* **29**, 16 (1955).
- [54] P. Ring and P. Schuck, *The Nuclear Many-Body Problem* (Springer Science & Business Media, Berlin, 2004).
- [55] P. W. Zhao, Z. P. Li, J. M. Yao, and J. Meng, *Phys. Rev. C* **82**, 054319 (2010).
- [56] S. G. Nilsson, C. F. Tsang, A. Sobczewski, Z. Szymański, S. Wycech, C. Gustafson, I.-L. Lamm, P. Möller, and B. Nilsson, *Nucl. Phys. A* **131**, 1 (1969).
- [57] Y. Y. Wang and Z. X. Ren, *Sci. China Phys. Mech. Astron.* **61**, 082012 (2018).
- [58] A. Bohr and B. R. Mottelson, *Nuclear Structure* (Benjamin, New York, 1975), Vol. 2.
- [59] C. Vaman, D. B. Fossan, T. Koike, K. Starosta, I. Y. Lee, and A. O. Macchiavelli, *Phys. Rev. Lett.* **92**, 032501 (2004).
- [60] Q. B. Chen and J. Meng, *Phys. Rev. C* **98**, 031303(R) (2018).